Underdense a-Si:H film capped by a dense film as the passivation layer of a silicon heterojunction solar cell

Wenzhu Liu,[1,2] Liping Zhang,[1] Renfang Chen,[1,2] Fanying Meng,[1] Wanwu Guo,[3] Jian Bao,[3] and Zhengxin Liu[1,a)]

[1]*Research Center for New Energy Technology (RCNET), Shanghai Institute of Microsystem and Information Technology (SIMIT), Chinese Academy of Sciences (CAS), Jiading, 201800 Shanghai, People's Republic of China*

[2]*University of Chinese Academy of Sciences (USAS), Shijingshan, 100049 Beijing, People's Republic of China*

[3]*State Key Laboratory of PV Sciences and Technology (SKL-PVST), Trinasolar, Changzhou, 213031 Jiangsu, People's Republic of China*

(Received 31 August 2016; accepted 20 October 2016; published online 3 November 2016)

Underdense hydrogenated amorphous silicon (a-Si:H) prepared by plasma-enhanced chemical vapor deposition was used as a passivation layer in silicon heterojunction (SHJ) solar cells. By reducing the thickness of the underdense a-Si:H passivation layer from 15 nm to 5 nm, the open circuit voltage (V_{oc}) of the corresponding SHJ solar cell increased significantly from 724.3 mV to 738.6 mV. For comparison, a widely used transition-zone a-Si:H passivation layer was also examined, but reducing its thickness from 15 nm to 5 nm resulted in a continuous V_{oc} reduction, from 724.1 mV to 704.3 mV. The highest efficiency was achieved using a 5-nm-thick underdense a-Si:H passivation layer. We propose that this advantageous property of underdense a-Si:H reflects its microstructural characteristics. While the porosity of a-Si:H layer enables H penetration into the amorphous network and the a-Si:H/c-Si interface, a high degree of disorder inhibits the formation of the epitaxial layer at the a-Si:H/c-Si interface during post-doping layer deposition. *Published by AIP Publishing.*
[http://dx.doi.org/10.1063/1.4966941]

I. INTRODUCTION

Hydrogenated amorphous silicon (a-Si:H) has attracted significant attention owing to its tunable electric and optical properties. This material has been successfully used in semiconductor and electrochemical devices such as amorphous silicon solar cells, amorphous/crystalline silicon heterojunction (SHJ) solar cells, and as the anode material in Li-ion batteries.[1–3] The most popular method for preparing a-Si:H has been chemical vapor deposition (CVD), including plasma-enhanced CVD (PECVD) and catalytic CVD (Cat-CVD). The former method is more suitable for mass production owing to its low energy consumption and resistance to metal contamination. The structure and characteristics of a-Si:H vary significantly, depending on the deposition conditions. For instance, a dangling bond density in the 10^{14}–10^{19} cm^{-3} range has been recorded using electron spin resonance (ESR).[4,5] In the 1980s, Sokrates demonstrated over-coordinated Si atoms in a-Si:H, i.e., fivefold-coordinated Si atoms containing floating bonds,[6,7] and these findings were used for interpreting the well-known Staebler–Wronski effect (SWE).[8,9] Furthermore, the density of bonded H has also been found to be distributed throughout a wide range, from 10^{20} cm^{-3} to 10^{22} cm^{-3}, homogeneous in the bulk and clustered in large voids.[10–12] Based on these discoveries and other characteristics such as doping effects,[13] it is rational to claim that a-Si:H alloys cannot be precisely described by the continuous random tetrahedral network (CRTN) model;[14] instead, these alloys contain discontinuous nanometer and sub-nanometer scale microstructures, such as microvoids and vacancies.[15] Owing to the broad range of deposition parameters, determining the conditions for obtaining an optimal a-Si:H remains challenging.

In particular, intrinsic a-Si:H films with a thickness in the 3–20 nm range are used for passivating the c-Si surface of SHJ solar cells.[16–18] Most previous research recommended the use of transition-zone a-Si:H films for saturating dangling bonds on the c-Si surface. However, in the present work, we found that the advantage of using transition-zone a-Si:H for passivating the c-Si surface of SHJ solar cells gradually diminishes and eventually becomes a disadvantage as the film thickness continuously decreases. Fortunately, when the thickness of the underdense a-Si:H passivation layer is gradually reduced, the efficiency of the SHJ solar cell continuously increases, by up to 6%. The microstructure and characteristics of a-Si:H strongly rely on the deposition conditions and particle bombardment.[19,20] We fabricated SHJ solar cells that were passivated using underdense and transition-zone a-Si:H films. The characteristics of these cells were systematically studied, to reveal the mechanism that underlies the advantageous characteristics of underdense a-Si:H passivation layers.

II. EXPERIMENTAL DETAILS

Intrinsic a-Si:H films with the thickness of ~20 nm were deposited on (100) float-zone (FZ) Si wafers (thickness, 525 ± 25 μm; resistivity, >3000 Ω·cm) and quartz glasses

a)Author to whom correspondence should be addressed. Electronic mail: z.x.liu@mail.sim.ac.cn

by PECVD, at a radio frequency of 13.56 MHz. Underdense a-Si:H (Film-Underdense, with low mass density and many large voids) was fabricated at 200 °C, 40 mW/cm^2, and 70 Pa, while Transition-zone a-Si:H (Film-Transition-zone, containing small Si crystallites confirmed by the Raman spectral analysis) was prepared at 200 °C, 17 mW/cm^2, and 20 Pa. As-deposited a-Si:H films on FZ Si substrates were measured using spectroscopic ellipsometry (SE; J. A. Woollam, M-2000XI); their thicknesses (d) and refractive indices (n_∞ in the $\lambda \to \infty$ limit) were obtained by fitting the measured (Ψ, Δ) with an optical model: a surface roughness layer/a-Si:H layer/c-Si substrate, during which the a-Si:H layer and the surface roughness layer adopted the Tauc-Lorentz model[21] and the Bruggeman effective medium approximation (BEMA; combining 50 vol. % bulk material with 50 vol. % ambient), respectively. Next, Si-H$_x$ infrared absorption was characterized by performing Fourier transform infrared spectroscopy (FTIR; Perkin Elmer, Spectrum 100), for estimating the hydrogen content (C_H).[15] Combining the derived d, n_∞, and C_H, mass densities of these a-Si:H thin films were determined according to the model proposed by Remeš *et al.*[22] Surface roughness values of these films were measured using atomic force microscopy (AFM) in the tapping mode. Cross-sectional images of Si substrates were acquired using high-resolution electron transmission microscopy (HR-TEM; FEI Tecnai TF-20), at a voltage of 200 kV. Raman spectra of quartz glass samples were recorded under a 514-nm-wavelength laser excitation. Weak glow-discharge H flux was intentionally used to bombard the films on the Si substrates, and this hydrogen plasma treatment (HPT) was conducted at 50 W and 200 Pa. Finally, Film-Underdense was measured using FTIR and Film-Transition-zone was analyzed using HR-TEM.

Two Czochralski (CZ) Si wafers (thickness, 180 μm; resistivity, 1–6 Ω·cm) were successively textured with an alkali solution, cleaned by the standard RCA process, and etched with a 2% HF solution. Next, the wafers were transferred to the PECVD chamber, where 15-nm-thick intrinsic a-Si:H films were deposited onto both their surfaces. The deposition conditions were the same as those for Film-Underdense and Film-Transition-zone, and are referred to as Passi-Underdense and Passi-Transition-zone, respectively. For both wafers, minority carrier lifetime (τ_{eff}) was measured using Sinton WCT-120 after the wafers cooled down to room temperature. Two types of SHJ solar cells were fabricated, with the following structure: 80-nm-thick tungsten-doped indium oxide layer/5-nm-thick B-doped a-Si:H layer/5-nm-thick intrinsic a-Si:H layer/c-Si substrate/5-nm-thick intrinsic a-Si:H layer/10-nm-thick P-doped a-Si:H layer/80-nm-thick tungsten-doped indium oxide layer. These cell types are referred to as Cell-Underdense and Cell-Transition-zone, and their passivation layer deposition conditions were identical to those of Film-Underdense and Film-Transition-zone, respectively. Silver electrodes with conventional finger and busbar patterns were screen-printed on these solar cells, followed by annealing at 200 °C for 30 min. The electric parameters were captured by a solar simulator under the standard condition (AM 1.5G, 25 °C). For convenience, the methods used for analyzing several cell types in the present work are summarized in Table I. Finally, two types of SHJ solar cells, with various passivation layer thicknesses, were fabricated using 110-μm-thick CZ Si wafers.

III. RESULTS AND DISCUSSION

A. Passivation quality of 15-nm-thick a-Si:H films

Fig. 1(a) shows the imaginary part (ε_2) of the dielectric function of Film-Transition-zone and Film-Underdense. The lower ε_2 peak in the case of Film-Underdense indicates that its mass density is smaller than that of Film-Transition-zone. Fig. 1(b) shows the FTIR spectra of the two films, revealing that Film-Underdense exhibits absorption dips at 845, 890, and 2084 cm^{-1}, which result from coupling between adjacent Si-H$_2$, Si-H$_2$ bending, and Si-H$_x$ high stretching modes.[23,24] This suggests the existence of large voids. This speculation is corroborated by the HR-TEM image in Fig. 3(e). Comparatively, the ε_2 curves and the FTIR spectra suggest that Film-transition-zone has a dense microstructure (transition-zone a-Si:H confirmed by the 505 cm^{-1} shoulder in the Raman spectrum in Fig. 3(c)). According to the optical model,[22,25] Film-Underdense has a mass density of 2.05 g/cm^3, substantially lower than that of Film-Transition-zone (2.23 g/cm^3). The schematic in Fig. 1(c) shows the sandwich structure of Passi-Underdense and Passi-Transition-zone. The τ_{eff} values (18 μs *vs.* 807 μs at an injection level of 1.0×10^{15} cm^{-3}) elucidate that the transition-zone a-Si:H material is more suitable for passivating c-Si than the underdense a-Si:H material.

Figs. 2(a) and 2(b) schematically show the SHJ solar cell and the I–V curves of Cell-Underdense and Cell-Transition-zone. The V_{oc} and fill factor (FF) values (727.4 mV and 78.4%, respectively) for Cell-Underdense are higher than those for Cell-Transition-zone (680.1 mV and 77.0%, respectively). Meanwhile, the J_{sc} values for the two scenarios are identical with respect to the temporal instability

TABLE I. Measurements and treatment of some samples in this work.

Samp. No.	SE	FTIR	AFM	Raman	HR-TEM	HPT	WCT-120	Solar simulator
Film-transition-zone	√	√	√	√	√	√		
Film-underdense	√	√	√	√	√	√		
Passi-transition-zone							√	
Passi-underdense							√	
Cell-transition-zone							√	√
Cell-underdense							√	√

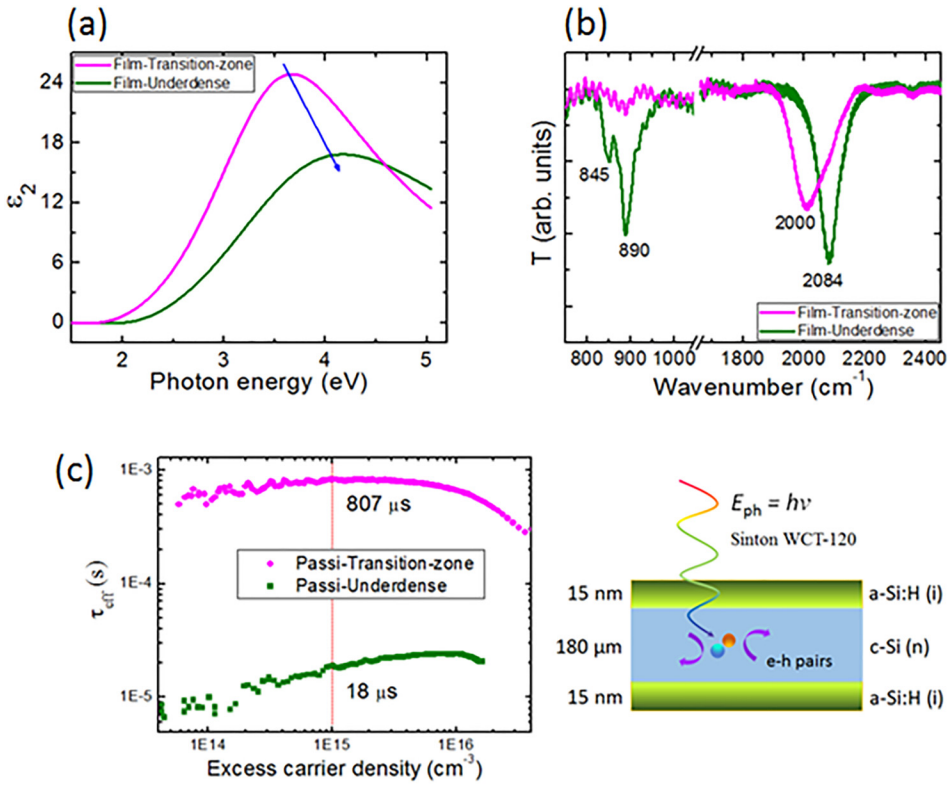

FIG. 1. (a) Imaginary parts (ε_2) of the dielectric functions and (b) FTIR spectra of Film-Transition-zone and Film-Underdense. (c) τ_{eff} curves of Passi-Transition-zone and Passi-Underdense.

of the solar simulator. This seemingly contradicts the results in Fig. 1(c), wherein the τ_{eff} values suggest that c-Si is less passivated by the underdense a-Si:H than by the transition-zone a-Si:H. However, Fig. 2(b) suggests that the electric performance of Cell-Underdense is better than that of Cell-Transition-zone. Theoretically, higher V_{oc} and FF indicate a lower density of defects at the a-Si:H/c-Si interface.[26,27] Comparing the τ_{eff} values in Fig. 1(c) with the *I–V* curves in Fig. 2(b), we conclude that the c-Si surfaces of Cell-Transition-zone were initially well-passivated by the transition-zone a-Si:H (implied open circuit voltage, $V_{oc\_imp} = 717$ mV), but the electric quality of the a-Si:H/c-Si interfaces deteriorated after depositing the densely doped a-Si:H layers onto the passivation layers ($V_{oc} = 680$ mV). Conversely, although the c-Si surfaces of Cell-Underdense were less passivated with the underdense a-Si:H layers ($V_{oc\_imp} = 550$ mV), the characteristics of the a-Si:H/c-Si interfaces improved after depositing the densely doped a-Si:H layers ($V_{oc} = 727$ mV). This indicates that the quality of the c-Si surface passivation is not completely determined by the passivation layer, with doped (B- and P-doped) a-Si:H layers also affecting the electrical properties at the interface.

B. Analysis of the passivation layer

Figs. 3(a) and 3(b) show the surface roughness plots of Film-Transition-zone and Film-Underdense, respectively. Numerous fine ~1-nm-tall bumps are observed on the surface of Film-Transition-zone, while the bumps on Film-Underdense are significantly prominent. Film growth rates of the Film-transition-zone and Film-Underdense were 0.9 Å/s and 4.3 Å/s, respectively. The chamber pressure and the SiH_4 flow rate were 20 Pa and 70 sccm during the deposition of Film-Transition-zone. Under such a low gas pressure and slow gas flow rate, SiH_4 molecules were relatively sufficiently dissociated. As a result, the plasma was dominated by small radicals and H atoms. The hopping frequency of small radicals on the film-growing surface was high, owing to their small weight. In addition, the high density of H guaranteed a full H coverage on the film-growing surface, which

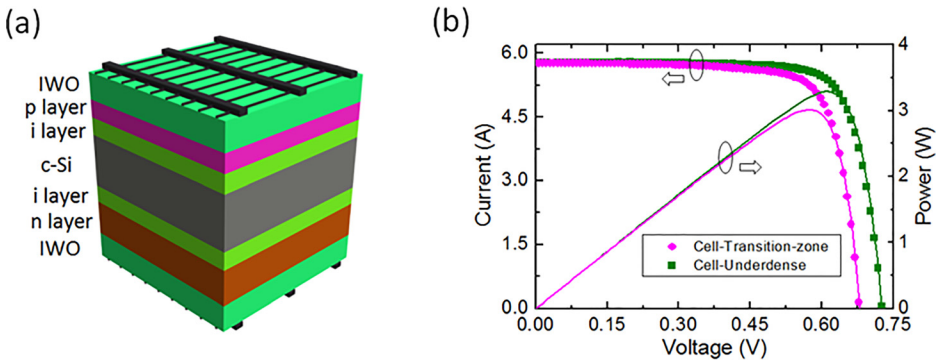

FIG. 2. (a) Schematic of the SHJ solar cell. (b) The *I–V* curves of Cell-Transition-zone and Cell-Underdense.

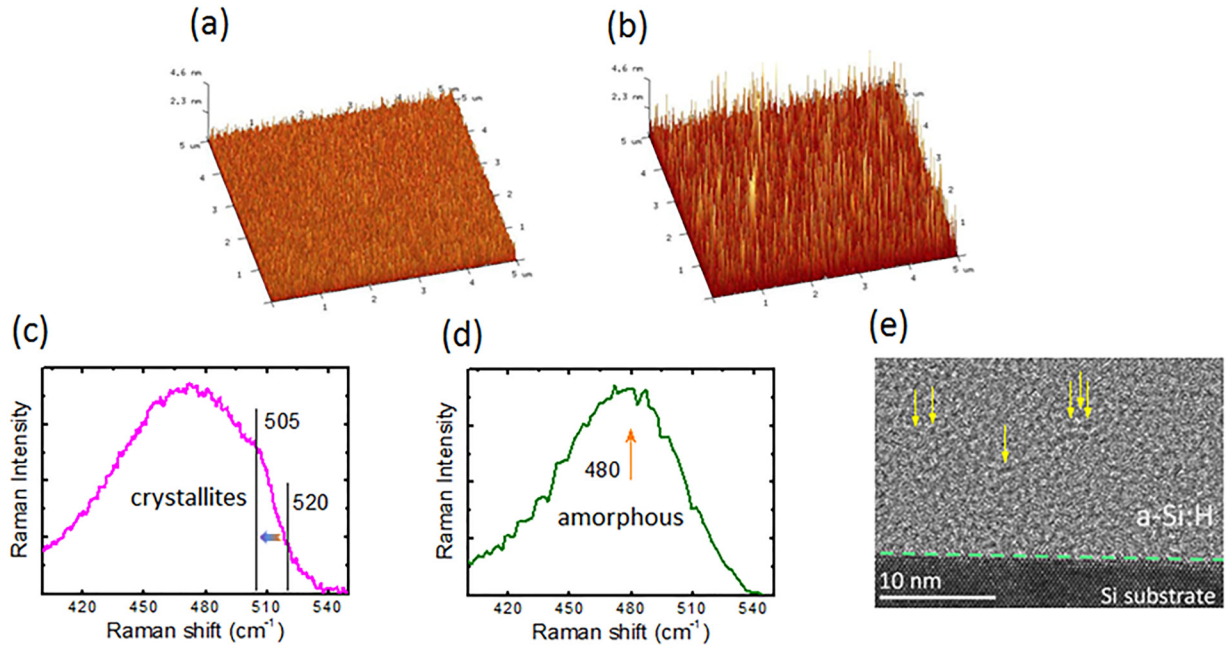

FIG. 3. Surface roughness of (a) Film-Transition-zone and (b) Film-Underdense. The Raman spectra of Film-Transition-zone and Film-Underdense are shown in (c) and (d), respectively. (e) The cross-sectional image of Film-Underdense, with some large voids marked by arrows.

was conducive to creating local heating via H-exchange reactions.[28] The released heat significantly enhanced the two-dimensional surface diffusion of film-growing radicals on the growing substrate. Consequently, film-growing radicals were very likely to reach energetically favorable sites, yielding the formation of a highly ordered Si network. This interpretation is supported by the 505 cm^{-1} Raman shift shoulder in Fig. 3(c), which was caused by small Si crystallites. For Film-Underdense, the deposition pressure and SiH_4 flow rate were 70 Pa and 150 sccm, respectively. Under such a high pressure and fast gas flow rate, a long-time deposition generated a yellow-brown powder in the chamber (not shown here), indicating the formation of large Si_xH_y molecules. The single Raman shift peak at 480 cm^{-1} in Fig. 3(d) suggests that Film-Underdense has a pure amorphous phase. Fig. 3(e) reveals the significant presence of large voids that are embedded in the amorphous network of Film-Underdense.

Fig. 4(a) shows the cross-sectional HR-TEM image of the as-deposited Film-Transition-zone. A small number of ordered Si atoms are observed at the a-Si:H/c-Si interface, but the epitaxial layer is not continuous and the thickness is below 1.3 nm. Fig. 4(b) shows the cross-sectional HR-TEM image of the Film-Transition-zone after the HPT, and it is found that the HPT induced a continuous thick epitaxial layer at the a-Si:H/c-Si interface. The H-induced network relaxation was caused by the insertion of H into strained Si-Si bonds as H atoms diffused through the transition-zone a-Si:H film.[29] Therefore, although transition-zone a-Si:H satisfactorily passivates the c-Si surface,[30] its microstructure is metastable and is easily changed by post H bombardment. Other groups have demonstrated that the epitaxial layer at the a-Si:H/c-Si interface is an important bulk defect source and only a-Si:H/c-Si with an abrupt interface can yield the most outstanding surface passivation.[31,32] Contrary to what is shown in Fig. 4(b), Fig. 3(e) shows that the underdense a-Si:H film exhibits a high degree of disorder, where the a-Si:H/c-Si interface is perfectly abrupt. Figs. 4(c) and 4(d) show the Si-H_x stretching absorption curves of Film-Underdense, before and after the HPT. The symmetrical peak in Fig. 4(c) results from clustered Si-H_x, and the absence of the low-frequency peak at ~2000 cm^{-1} suggests that the bulk material of as-deposited Film-Underdense is short of bonded H. However, the low-frequency peak appeared after the HPT (Fig. 4(d)), during which a portion of strained Si-Si bonds was split up, yielding the bulk Si-H bond formation. This is the evidence of H penetration into the underdense passivation layer. It is well known that mobile H provided by a-Si:H is necessary for passivating the a-Si:H/c-Si interface. However, if the structure-loose a-Si:H of Passi-Underdense is not capped with a densely doped a-Si:H layer, the temperature step may induce H mobility in the a-Si:H passivation layer, which helps H to escape towards a vacuum. This can explain why the τ_{eff} of Passi-Underdense is so short (Fig. 1(c)) but the performance of Cell-Underdense is excellent (Fig. 2(b)). We would like to emphasize that the cross-sectional image of Film-Underdense was not characterized because there is a high density of large voids in this sample (Fig. 3(e)). For such a serious mass deficiency, a-Si:H was extremely difficult to crystallize. The abrupt a-Si:H/c-Si interface can also be corroborated by the good performance of SHJ solar cells with underdense passivation layers in Fig. 5.

C. Influence of the passivation layer thickness on the SHJ solar cell characteristics

Fig. 5 shows the plots of electrical characteristics vs. the passivation layer thickness, for two groups of SHJ solar cells with passivation-layer deposition conditions the same as those of the Film-Transition-zone and Film-Underdense. When transition-zone passivation layer thickness decreased from 15 nm to 5 nm (indicated by the squares), the J_{sc} and

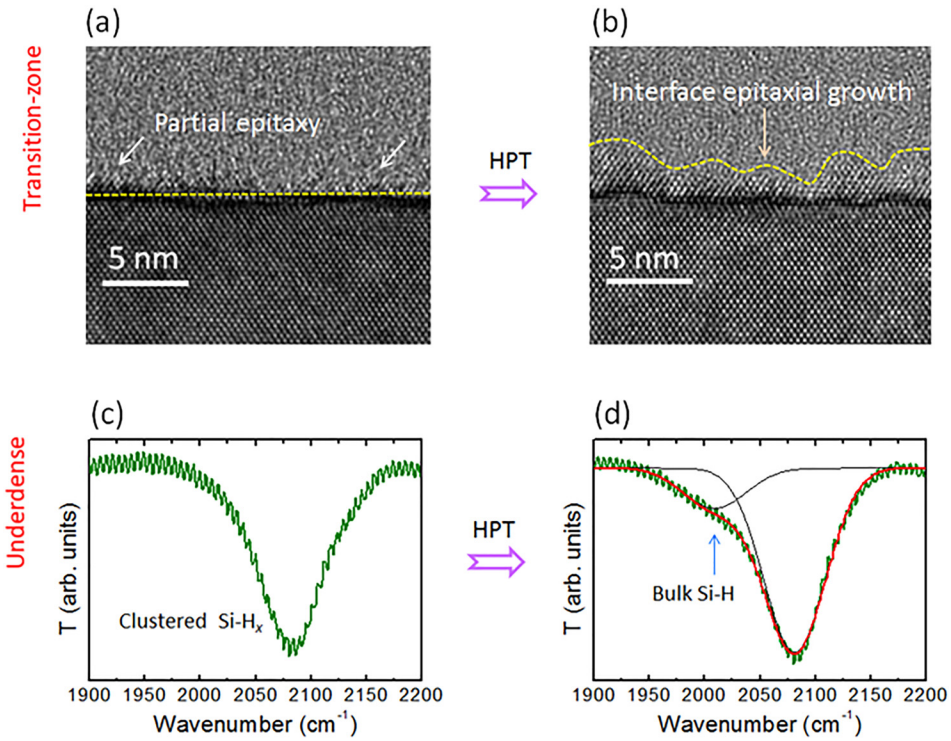

FIG. 4. Interface HR-TEM images of Film-Transition-zone (a) before and (b) after HPT, and the FTIR spectra of Film-Underdense (c) before and (d) after HPT.

FF (Figs. 5(a) and 5(c)) increased and then tended to saturate. This was attributed to the reduction in the series resistance. However, V_{oc} (Fig. 5(b)) decreased continuously from 724.1 mV to 704.3 mV, counteracting the enhancement in J_{sc} and FF. As a consequence, the cell efficiency increased slightly from 20.8% to 21.4%, but then decreased to 20.9% (Fig. 5(d)). Referring to the above-mentioned HPT experiment, we speculate that the V_{oc} decay was caused by the epitaxial layer at the a-Si:H/c-Si interface. In this case, the epitaxial layer was probably formed by H

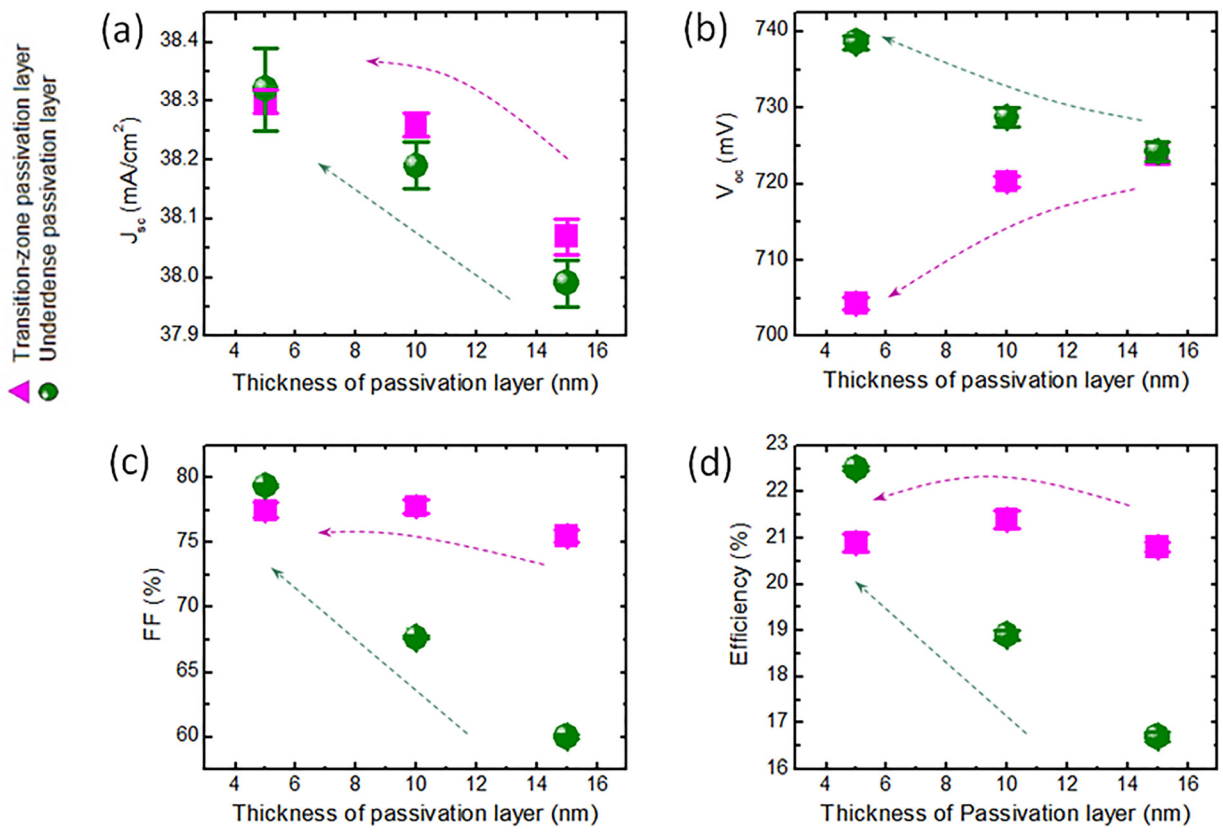

FIG. 5. (a) J_{sc}, (b) V_{oc}, (c) FF, and (d) efficiency of SHJ solar cells, vs. the passivation layer thickness, for deposition conditions identical to those of Film-Transition-zone (squares) and Film-Underdense (circles).

bombardment during the deposition of the densely doped a-Si:H layer. The thinner the passivation layer, the more the kinetic H atoms could arrive at the partial a-Si:H/c-Si interface, yielding a thicker epitaxial layer. This rationalizes the continuous V_{oc} decay with decreasing thickness of the passivation layer in Fig. 5(b). On the other hand, for SHJ solar cells passivated by underdense a-Si:H (circles), Figs. 5(a)–5(c) reveal that reducing the passivation layer's thickness improved the J_{sc}, V_{oc}, and FF characteristics. Accordingly, the efficiency also increased from 16.7% to 22.5% (Fig. 5(d)). Analysis of the SE measurement revealed that the disorder parameter C was 2.5 for Film-Underdense, higher than the value of 2.1 for the Film-Transition-zone. On the one hand, such a strongly disordered amorphous network with the significant presence of large voids (Fig. 3(e)) is difficult to crystallize because much more energy is needed to achieve the network relaxation. On the other hand, H penetration during capping densely doped a-Si:H layers reduces the density of defects in the a-Si:H passivation layer and at the a-Si:H/c-Si interface, and for thinner passivation layers, more H atoms reached the a-Si:H/c-Si interface. Furthermore, the densely doped a-Si:H suppressed the escape of H from the structure-loose passivation layer caused by a temperature step. This explains the enhancement of V_{oc} with the decrease in the passivation layer's thickness, as shown in Fig. 5(b). Fig. 5(d) also reveals that for passivation layers thicker than ~7 nm, transition-zone a-Si:H yields better passivation than underdense a-Si:H, but for passivation layers thinner than ~7 nm, underdense a-Si:H yields better passivation. The highest efficiency was achieved for a 5-nm-thick underdense a-Si:H passivation layer.

IV. CONCLUSIONS

We demonstrated that underdense a-Si:H performs better than transition-zone a-Si:H when these ultrathin films are used for passivating the c-Si surfaces of SHJ solar cells. For ultrathin transition-zone a-Si:H films on c-Si, insertion of kinetic H atoms during capping of densely doped a-Si:H layers may result in epitaxial Si growth and thus lead to a high density of defects at the a-Si:H/c-Si interface. This substantially affects V_{oc} of the corresponding SHJ solar cell. In contrast, underdense a-Si:H exhibits a highly disordered microstructure and contains such a high density of large voids that an abrupt a-Si:H/c-Si interface is obtained when it is deposited onto a c-Si substrate. The penetration of H during the deposition of densely doped a-Si:H layers can secondarily passivate the a-Si:H/c-Si interface without affecting the abruptness of the a-Si:H/c-Si interface, therefore achieving higher SHJ solar cell efficiency.

ACKNOWLEDGMENTS

The authors acknowledge Mr. Ziwen Wang and Mr. Pengfei Jia for the AFM measurements. This work was supported by the Main Direction Program of Knowledge Innovation of the Chinese Academy of Sciences (No. KGCX2-YW-399+11), the National High Technology Research and Development Program of China (863 Program, No. 2011AA050501), the International S&T Cooperation Program of China (No. 2015DFA60570), and the Innovation Development Fund of Shanghai (No. ZJ2015-ZD-001).

[1]D. E. Carlson and C. R. Wronski, Appl. Phys. Lett. **28**, 671 (1976).
[2]K. Masuko, M. Shigematsu, T. Hashiguchi, D. Fujishima, M. Kai, N. Yoshimura, T. Yamaguchi, Y. Ichihashi, T. Mishima, N. Matsubara, T. Yamanishi, T. Takahama, M. Taguchi, E. Maruyama, and S. Okamoto, IEEE J. Photovoltaics **4**, 1433 (2014).
[3]S. Bourderau, T. Brousse, and D. M. Schleich, J. Power Sources **81–82**, 233 (1999).
[4]R. A. Street and K. Winer, Phys. Rev. B **40**, 6236 (1989).
[5]Y. Wu, J. T. Stephen, D. X. Han, J. M. Rutland, R. S. Crandall, and A. H. Mahan, Phys. Rev. Lett. **77**, 2049 (1996).
[6]S. T. Pantelides, Phys. Rev. Lett. **57**, 2979 (1986).
[7]S. T. Pantelides, Phys. Rev. Lett. **58**, 1344 (1987).
[8]M. Stutzmann, W. B. Jackson, and C. C. Tsai, Appl. Phys. Lett. **45**, 1075 (1984).
[9]H. Fritzsche, Solid State Commun. **94**, 953 (1995).
[10]A. A. Langford, M. L. Fleet, B. P. Nelson, W. A. Lanford, and N. Maley, Phys. Rev. B **45**, 13367 (1992).
[11]A. H. Mahan, J. Carapella, B. P. Nelson, R. S. Crandall, and I. Balberg, J. Appl. Phys. **69**, 6728 (1991).
[12]S. Gerke, H. W. Becker, D. Rogalla, F. Singer, N. Brinkmann, S. Fritz, A. Hammud, P. Keller, D. Skorka, D. Sommer, C. Weiß, S. Flege, G. Hahn, R. Job, and B. Terheiden, Thin Solid Films **598**, 161 (2016).
[13]M. Stutzmann, D. K. Biegelsen, and R. A. Street, Phys. Rev. B **35**, 5666 (1987).
[14]W. Y. Ching, C. C. Lin, and L. Guttman, Phys. Rev. B **16**, 5488 (1977).
[15]A. H. M. Smets, W. M. M. Kessels, and M. C. M. van de Sanden, Appl. Phys. Lett. **82**, 1547 (2003).
[16]S. K. Kim, J. C. Lee, S. J. Park, Y. J. Kim, and K. H. Yoon, Sol. Energy Mater. Sol. Cells **92**, 298 (2008).
[17]Y. Tsunomura, Y. Yoshimine, M. Taguchi, T. Baba, T. Kinoshita, H. Kanno, H. Sakata, E. Maruyama, and M. Tanaka, Sol. Energy Mater. Sol. Cells **93**, 670 (2009).
[18]V. A. Dao, J. Heo, H. Choi, Y. Kim, S. Park, S. Jung, N. Lakshminarayan, and J. Yi, Sol. Energy **84**, 777 (2010).
[19]A. Illiberi, P. Kudlacek, A. H. M. Smets, M. Creatore, and M. C. M. van de Sanden, Appl. Phys. Lett. **98**, 242115 (2011).
[20]G. Dingemans, M. N. van den Donker, D. Hrunski, A. Gordijn, W. M. M. Kessels, and M. C. M. van de Sanden, Appl. Phys. Lett. **93**, 111914 (2008).
[21]G. E. Jellison and F. A. Modine, Appl. Phys. Lett. **69**, 371 (1996).
[22]Z. Remes, M. Vanecek, P. Torres, U. Kroll, A. H. Mahan, and R. S. Crandall, J. Non-Cryst. Solids **227**, 876 (1998).
[23]M. Cardona, Phys. Status Solidi B **118**, 463 (1983).
[24]A. H. M. Smets and M. C. M. van de Sanden, Phys. Rev. B **76**, 073202–1 (2007).
[25]W. Liu, L. Zhang, F. Meng, W. Guo, J. Bao, J. Liu, D. Wang, and Z. Liu, Scr. Mater. **107**, 50 (2015).
[26]H. Li, X. B. Zeng, X. B. Xie, P. Yang, J. Y. Li, X. D. Zhang, and Q. M. Wang, Adv. Mater. Res. **773**, 124 (2013).
[27]X. Wen, X. Zeng, W. Liao, Q. Lei, and S. Yin, Sol. Energy **96**, 168 (2013).
[28]A. Matsuda, Jpn. J. Appl. Phys., Part 1 **43**, 7909 (2004).
[29]S. Sriraman, S. Agarwal, E. S. Aydil, and D. Maroudas, Nature **418**, 62 (2002).
[30]J. Ge, Z. P. Ling, J. Wong, R. Stangl, A. G. Aberle, and T. Mueller, J. Appl. Phys. **113**, 234310 (2013).
[31]T. H. Wang, E. Iwaniczko, M. R. Page, D. H. Levi, Y. Yan, H. M. Branz, and Q. Wang, Thin Solid Films **501**, 284 (2006).
[32]S. D. Wolf and M. Kondo, Appl. Phys. Lett. **90**, 042111 (2007).